

Calibrated Feature Decomposition for Generalizable Person Re-Identification

Kecheng Zheng, Jiawei Liu, Wei Wu, Liang Li, Zheng-jun Zha

University of Science and Technology of China

zkcys001@mail.ustc.edu.cn

Abstract

Existing disentangled-based methods for generalizable person re-identification aim at directly disentangling person representations into domain-relevant interference and identity-relevant feature. However, they ignore that some crucial characteristics are stubbornly entwined in both the domain-relevant interference and identity-relevant feature, which are intractable to decompose in an unsupervised manner. In this paper, we propose a simple yet effective Calibrated Feature Decomposition (CFD) module that focuses on improving the generalization capacity for person re-identification through a more judicious feature decomposition and reinforcement strategy. Specifically, a calibrated-and-standardized Batch normalization (CSBN) is designed to learn calibrated person representation by jointly exploring intra-domain calibration and inter-domain standardization of multi-source domain features. CSBN restricts instance-level inconsistency of feature distribution for each domain and captures intrinsic domain-level specific statistics. The calibrated person representation is subtly decomposed into the identity-relevant feature, domain feature, and the remaining entangled one. For enhancing the generalization ability and ensuring high discrimination of the identity-relevant feature, a calibrated instance normalization (CIN) is introduced to enforce discriminative id-relevant information, and filter out id-irrelevant information, and meanwhile the rich complementary clues from the remaining entangled feature are further employed to strengthen it. Extensive experiments demonstrate the strong generalization capability of our framework. Our models empowered by CFD modules significantly outperform the state-of-the-art domain generalization approaches on multiple widely-used benchmarks. Code will be made public: <https://github.com/zkcys001/CFD>.

1. Introduction

Person Re-identification (re-id) [33, 39, 42, 47] has achieved remarkable success under the transductive domain adaptive setting with the assumption that training and test-

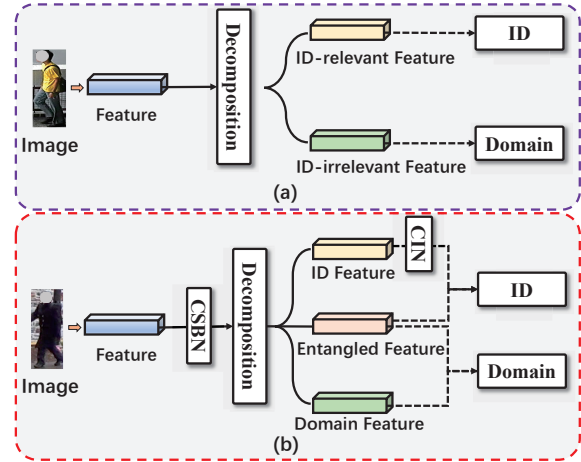


Figure 1. Illustration of motivation and our idea. (a) Conventional disentangled-based ReID method. They often make the strong assumption that the person representation can be decomposed into the id-relevant feature and id-irrelevant feature, and they also ignore to adopt a suitable reinforcement strategy as the guidance of feature decomposition; (b) Our proposed CDM module proposes a more judicious decomposition strategy to decompose person representation into the identity-relevant feature, domain feature, and the remaining entangled one. Meanwhile, we also adopt the CSBN and CIN to facilitate feature decomposition.

ing data are easily collected. However, this assumption is often violated in practical applications, as new domain data are not always accessible due to privacy issues and expensive labeling costs, which causes dramatic performance degradation on the unseen target domain. For example, the model trained on the data collected in the daytime domain performs poorly on unseen nighttime domains. Therefore, recent efforts have been devoted to Domain Generalizable Person Re-Identification (dubbed as DG-ReID) problem that aims to learn a general domain-agnostic model, which can generalize well to unseen target domains.

Although plenty of domain generalization methods [4, 17] (i.e., data manipulation, representation learning and learning strategy) are proposed, they have been often confined to the situation that the source and target domains share the same label space with a fixed amount of classes.

In contrast, domain generalization for person Re-ID is an open-set retrieval task, having different and variable numbers of identities between source and target domains. Therefore, it is difficult to achieve satisfying generalization capability when the existing DG approaches are directly applied to person Re-ID.

To address this problem, several tailored DG-ReID methods [6, 7, 14, 28, 31, 32, 43, 53] have been proposed, which can be mainly divided into three categories: meta-learning based model, ensemble learning based model and disentanglement based model. Ensemble learning based methods [7, 28, 31, 53] assemble multiple domain specific models like experts or classifiers to enhance the generalization ability of the overall network. Meta-learning based models [6, 43] combine a model-agnostic meta learning with the normalization technology to mimic real train-test domain shift for improving the generalization of the model. Normalization technique plays an important role in domain generalization task, because it can eliminate id-irrelevant discrepancy to restore helpful discriminative information. Nevertheless, these methods fail to deeply analyze the impact of different types of normalization techniques placed in different positions on the corresponding features. Meanwhile, these two kinds of methods significantly enlarge model complexity as the number of source domains increases during training.

Compared to the two types of aforementioned methods, as illustrated in Fig. 1 (a), the disentanglement based model is a more straightforward and efficient approach for DG-ReID [10, 20, 40, 41, 54]. It aims to directly disentangle identity-irrelevant interference and domain-invariant feature from the learned representations, and employ the domain-invariant feature to improve the generalization. However, these methods do not jointly consider the instance-level inconsistency of feature distribution within each domain and intrinsic domain-level specific statistics [11], which undermine the inherent relevance of unseen target domain with respect to source domains, resulting in unsatisfying generalization capability. Such instance-level inconsistency [6, 11, 16] and domain-specific characteristics [3, 9, 29, 31] can provide adequately discriminative and meaningful information, and guide the model to enable better feature decomposition from the perspective of improving the model generalization. More importantly, these disentanglement based methods ignore that some crucial characteristics are stubbornly entwined in both the domain-relevant interference and identity-relevant feature, which are intractable to decompose in an unsupervised manner. The object of this task is to improve the generalization of the model rather than to perform a complete feature disentanglement. Thus, it is more judicious to decompose the person representation into the identity-relevant feature, domain feature, and the remaining entangled one, and apply

suitable normalization techniques to the corresponding features for improving model generalization. This judicious feature decomposition with a suitable reinforcement strategy is the key to the success of DG-ReID.

In this architecture, we propose a simple yet effective Calibrated Feature Decomposition module that focuses on improving the generalization capacity for person re-identification through a more judicious feature decomposition and reinforcement strategy. Specifically, in the CFD module, we first employ a CSBN to learn calibrated person representation by jointly exploring intra-domain calibration and inter-domain standardization of multi-source domain features. CSBN restricts instance-level inconsistency of feature distribution within each domain and captures intrinsic domain-level specific statistics. Then we utilize a more judicious feature decomposition to subtly decompose the above calibrated person representation into identity-relevant feature, domain feature, and the remaining entangled one. For enhancing the generalization ability and ensuring high discrimination of identity-relevant feature, CIN is introduced to enforce discriminative id-relevant information and filter out id-irrelevant information. However, such a process inevitably ignores the entangled id-related information, we consider employing the rich complementary clues from the remaining entangled feature to strengthen the id-relevant feature. In addition, domain loss is employed to ensure that id-irrelevant domain information does not flow into the subsequent network. Extensive experiments demonstrate the strong generalization capability of our framework. Our models empowered by the CFD modules significantly outperform the state-of-the-art domain generalization approaches on multiple widely-used person ReID benchmarks.

The main contributions of this paper are as following:

- We propose a domain generalizable person ReID method that generalizes well on unseen domains. Particularly, we design a Calibrated Feature Decomposition module, which is simple yet effective and can be used as a plug-and-play module for existing ReID architectures to enhance their generalization capability.
- Our CDM module has a more judicious feature decomposition for enhancement of model generalization capabilities, which subtly decompose the person representation into the identity-relevant feature, domain feature, and the remaining entangled one.
- We propose two simple yet effective normalization-based reinforcement strategies that complement each other to improve the generalization and robustness of the model. CSBN is adopted to learn calibrated person representation by jointly exploring intra-domain calibration and inter-domain standardization of multi-source domain features; CIN is used to eliminate some

style discrepancies followed by entangled identity-relevant information restitution.

2. Related Work

2.1. Domain Generalizable Re-IDentification

Generalization capability to unseen domains is crucial for person re-id models when deploying to practical applications. To address this problem, several tailored DG-ReID methods [6, 7, 25, 28, 31, 32, 43, 53] have been proposed, which can be mainly divided into three categories: meta-learning based model, ensemble learning based model and disentanglement based model. Due to the success of disentangled learning, the DG-ReID methods based on disentangled learning [10, 20, 41, 54] improve the model generalization ability by disentangling person representations into identity-irrelevant interference and id-invariant feature. Specifically, Eom *et al.* [10] propose to disentangle identity-related and -unrelated features from person images and adopt identity shuffle GAN to enhance the person representation. Zhang *et al.* [41] propose a Disentanglement-based Cross-Domain Feature Augmentation (DCDFA) strategy to generate virtual samples in the feature space by adding disentangled domain-specific enhancements upon disentangled domain-shared identity bases. Zhang *et al.* [40] construct a structural causal model (SCM) to disentangle the person representation into identity-specific factors and domain-specific factors. Jin *et al.* [20] design the Style Normalization and Restitution (SNR) module based on instance normalization and feature distillation. However, these disentanglement based models ignore that some crucial characteristics are stubbornly entwined in both the domain-relevant interference and identity-relevant feature, which are intractable to decompose in an unsupervised manner. The goal of DG-ReID is to improve the generalization of the model rather than to perform a complete feature disentanglement. Thus, a more judicious feature decomposition with a suitable reinforcement strategy is important for the success of DG-ReID.

2.2. Normalization in DA and DG

Normalization techniques in deep neural networks are designed for regularizing trained models and improving their generalization performance. Recently, several methods on domain adaptation (DA) and domain generalization (DG) discovered the relationship between domain gap and normalization operation. For example, Jin *et al.* [19] proposed a Style Normalization and Restitution module, which utilizes the Instance Normalization (IN) layers to filter out style variations and compensates for the identity-relevant features discarded by IN layers. Seo *et al.* [31] proposed to leverage instance normalization to optimize the trade-off between cross-category variance and domain invariance,

which is desirable for domain generalization in unseen domains. Zhuang *et al.* [53] proposed camera-based batch normalization (CBN) to force the images of all cameras to fall onto the same subspace and to shrink the distribution gap between any camera pair.

3. Approach

Overview. Fig. 2 shows the overall architecture of our framework. In this architecture, we propose a simple yet effective Calibrated Feature Decomposition (CFD) module that focuses on improving the generalization capacity for person re-identification through a more judicious feature decomposition and reinforcement strategy. Taking the widely used ResNet-50 [13] in ReID network as a backbone, CFD module as a plug-and-play technology can be easily added after each convolutional block and is extremely easy to implement. Specifically, in the CFD module, we first employ a CSBN to learn calibrated person representation by jointly exploring intra-domain calibration and inter-domain standardization of multi-source domain features. CSBN restricts instance-level inconsistency of feature distribution for each domain and captures intrinsic domain-level specific statistics. Then we utilize a more judicious feature decomposition to subtly decompose the above calibrated person representation into the identity-relevant feature, domain feature, and the remaining entangled one. For enhancing the generalization ability and ensuring high discrimination of identity-relevant feature, CIN is introduced to enforce discriminative id-relevant information and filter out id-irrelevant information. However, such a process inevitably ignores the entangled id-related information, we consider employing the rich complementary clues from the remaining entangled feature to strengthen id-relevant information. In addition, a domain loss is used to ensure that id-irrelevant domain information does not flow into the subsequent network.

We aim at constructing an efficient, generalizable, and robust person ReID framework for the domain generalizable person re-identification task.

3.1. Calibrated Feature Decomposition (CFD)

In this section, we firstly introduce the novel feature decomposition mechanism for DG re-ID. For a CFD module, we denote the input that is from the ResNet Block by $\mathbf{F} \in \mathbb{R}^{h \times w \times c}$, and the outputs by $\mathbf{R}^I, \mathbf{R}^D \in \mathbb{R}^{h \times w \times c}$, where h, w, c denote the height, width, and number of channels, respectively.

Given \mathbf{F} from one ResNet Block, we firstly employ a CSBN to learn calibrated person representation $\tilde{\mathbf{F}}$ by jointly exploring intra-domain calibration and inter-domain standardization of multi-source domain features. Then, this calibrated person representation $\tilde{\mathbf{F}}$ is decomposed into two parts: soft entangled feature $\mathbf{R} \in \mathbb{R}^{h \times w \times c}$

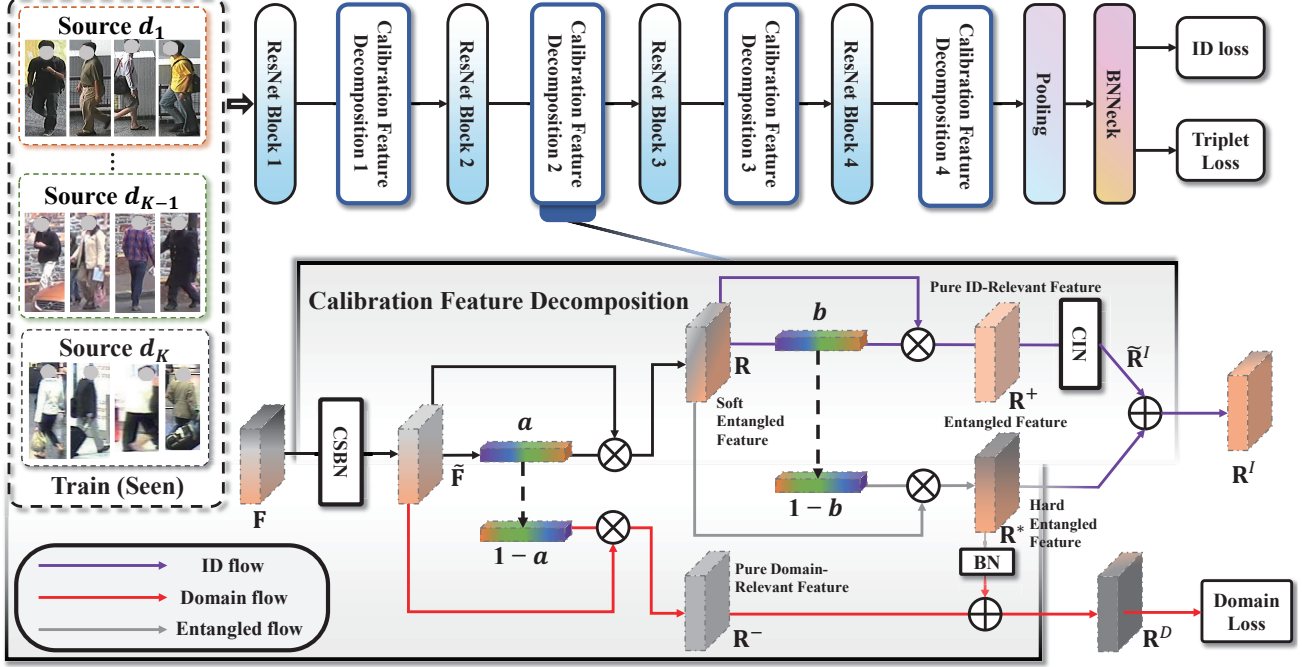


Figure 2. Overall flowchart. (a) Our generalizable person ReID network with the proposed CDM module being plugged in after some convolutional blocks. Here, we use ResNet-50 as our backbone for illustration. (b) The proposed CFD module. The calibrated-and-standardized Batch normalization is designed to learn calibrated person representation by jointly exploring intra-domain calibration and inter-domain standardization of multi-source domain features. A calibrated instance normalization is introduced to enforce discriminative id-relevant information and filter out id-irrelevant information, and meanwhile the rich complementary clues from the remaining entangled feature are further employed to strengthen it.

and pure domain-relevant feature $\mathbf{R}^- \in \mathbb{R}^{h \times w \times c}$ (i.e., this feature contains the domain information that is irrelevant to id information). To adequately filter out this pure domain-relevant feature \mathbf{R}^- , following the previous disentanglement-based ReID methods [20, 41], we utilize learnable channel attention vector $\mathbf{a} = [a_1, a_2, \dots, a_c] \in \mathbb{R}^c$ for soft feature decomposition:

$$\begin{aligned} \mathbf{R}(:, :, k) &= a_k \tilde{\mathbf{F}}(:, :, k), \\ \mathbf{R}^-(:, :, k) &= (1 - a_k) \tilde{\mathbf{F}}(:, :, k), \end{aligned} \quad (1)$$

where $\mathbf{R} \in \mathbb{R}^{h \times w \times c}$ refers to the soft entangled feature, consisting of the pure identity-relevant feature and hard entangled feature. We expect that the channel attention vector \mathbf{a} to enable the adaptive distillation of the domain-relevant features for filtering out the id-unrelated feature, and derive it by channel attention as:

$$\mathbf{a} = g(\tilde{\mathbf{F}}) = \sigma(\mathbf{W}_2 \cdot \delta(\mathbf{W}_1 \cdot \text{pool}(\tilde{\mathbf{F}}))), \quad (2)$$

where $\text{pool}(\cdot)$ refers to a global average pooling layer followed by two fully-connected layers that are parameterized by $\mathbf{W}_2 \in \mathbb{R}^{(c/r) \times c}$ and $\mathbf{W}_1 \in \mathbb{R}^{c \times (c/r)}$. ReLU $\delta(\cdot)$ and sigmoid $\sigma(\cdot)$ are utilized as the activation function, respec-

tively. In addition, a dimension reduction ratio r is used to reduce the number of parameter and is set to 16.

In a same way, for distilling the better id-relevant information, we also adopt the channel attention to decompose the soft entangled feature \mathbf{R} into hard entangled feature $\mathbf{R}^* \in \mathbb{R}^{h \times w \times c}$ and pure id-relevant feature $\mathbf{R}^+ \in \mathbb{R}^{h \times w \times c}$:

$$\begin{aligned} \mathbf{R}^*(:, :, k) &= b_k \mathbf{R}(:, :, k), \\ \mathbf{R}^+(:, :, k) &= (1 - b_k) \mathbf{R}(:, :, k), \end{aligned} \quad (3)$$

To enforce discriminative id-relevant information and filter out id-irrelevant information, a CIN is employed to the \mathbf{R}^+ to obtain the calibrated pure id-relevant feature $\tilde{\mathbf{R}}^+$, and meanwhile the rich complementary clues from the remaining entangled feature \mathbf{R}^* is further employed to strengthen $\tilde{\mathbf{R}}^+$. Moreover, to ensure that id-irrelevant domain information does not flow into the main branch as much as possible, we also add hard entangled feature \mathbf{R}^* into pure domain-relevant feature \mathbf{R}^- , and use the domain classification loss to guide the output feature \mathbf{R}^D :

$$\begin{aligned} \mathbf{R}^I &= \tilde{\mathbf{R}}^+ + \mathbf{R}^*, \\ \mathbf{R}^D &= \mathbf{R}^- + \mathbf{R}^*, \end{aligned} \quad (4)$$

where \mathbf{R}^I refers to the discriminative identity-relevant fea-

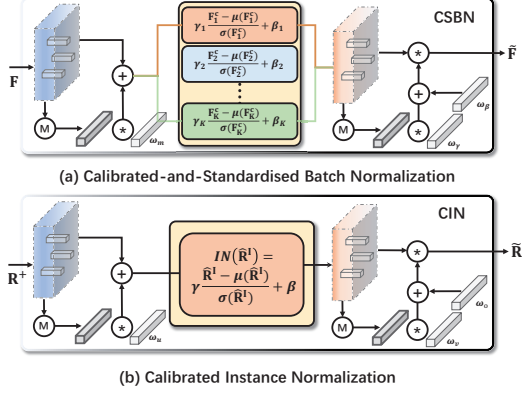


Figure 3. The details of the calibrated-and-standardized batch normalization and the calibrated instance normalization.

feature, and \mathbf{R}^D refers to the contributive domain-relevant feature. A few factors of person representations simultaneously are twined in both the domain-relevant interference and identity-relevant feature, which are intractable to decompose. Our goal is to obtain a more generalizable pedestrian feature rather than to have the feature decoupled. So, it is more important to filter out the id-irrelevant feature, and enhance the discrimination of id-related feature, where this strategy is more suitable for DG re-ID.

3.2. Calibrated Normalization.

Calibrated-standardized Batch Normalization. Previous Batch Normalization (BN), Instance Normalization (IN), or other normalization technologies do not jointly consider intra-domain calibration and inter-domain standardization of multi-source domain features. However, the instance-level inconsistency of feature distribution for each domain and intrinsic domain-level specific statistics are beneficial for the generalization ability of model [9, 11]. Thus, to enable the intra-domain calibration, we add a centering calibration scheme driven by instance statistics, where the centering calibration is added before BN layer. Given input feature \mathbf{F} , the centering calibration of features is written as follows:

$$\mathbf{F}^c = \mathbf{F} + \omega_m \odot \text{pool}(\mathbf{F}) \quad (5)$$

where $\text{pool}(\cdot)$ refers to a max average pooling layer and ω_m is the shared learnable weight vector between domains. \odot refers to the dot product, which broadcasts two features to the same dimension size and then conducts dot product.

Because the distribution of different domains varies widely, using a regular BN upon all source domains would result in confusing statistical information. And sharing parameters across multiple domains is inappropriate due to the existence of a domain gap. Inspired by [9], we use domain-specific BN to enable inter-domain standardization of multi-source domain features. When testing, we adopt the mean path of BN parameters to extract the unseen domain feature,

which enables better generalization ability. Specifically, let $\mathbf{F}^c = (\mathbf{F}_1^c, \mathbf{F}_2^c, \dots, \mathbf{F}_K^c)$ denotes feature maps of the centering calibrated representation including K domains, CSBN module can be written as:

$$\begin{aligned} \tilde{\mathbf{F}}_k &= \text{CSBN}(\mathbf{R}^I) \\ &= (\gamma_d \frac{\mathbf{F}_k^c - \mu(\mathbf{F}_d^c)}{\sigma(\mathbf{F}_k^c)} + \beta_d) \cdot \text{Sigmoid}(\omega_\gamma \odot \mathbf{F}_k^c + \omega_\beta), \end{aligned} \quad (6)$$

where $\tilde{\mathbf{F}} = (\tilde{\mathbf{F}}_1, \tilde{\mathbf{F}}_2, \dots, \tilde{\mathbf{F}}_K)$, $\tilde{\mathbf{F}}_k$ denotes the calibrated person representation of k-th domain, $\omega_\gamma, \omega_\beta$ are shared learnable weight vectors between domains, β_d, β_d are individual learnable weight vectors in each domain, and $\text{Sigmoid}(\cdot)$ means regular sigmoid activation function. The calibrated-and-standardized Batch normalization in CFD jointly explores intra-domain calibration and inter-domain standardization of multi-source domain features to perform calibrated feature normalization. Specifically, we utilize the ω_m, ω_γ and ω_β are shared learnable weight vectors between domains to perform intra-domain calibration. Then, the domain-specific individual parameters (*i.e.*, β_d, β_d) are adopted for the inter-domain standardization.

Calibrated Instance Normalization In previous methods [8, 16, 35], they try to reduce the domain discrepancy on the input features by performing IN as:

$$\tilde{\mathbf{R}}^I = \text{IN}(\mathbf{R}^I) = \gamma(\frac{\mathbf{R}^I - \mu(\mathbf{R}^I)}{\sigma(\mathbf{R}^I)}) + \beta, \quad (7)$$

where $\mu(\cdot)$ and $\sigma(\cdot)$ denote the mean and standard deviation computed across spatial dimensions independently for each channel and each *sample/instance*, $\gamma, \beta \in \mathbb{R}^c$ are parameters learned from data. IN could filter out some instance-specific style information from the content. But the correct placement of IN is also not considered in the previous decoupling method [10, 20, 39]. Because of the nature of IN [8, 16, 35], we put it in the pure ID-related features to better perceive the ID-relevant information from entangled feature. In addition, for enhancing the generalization ability and ensuring high discrimination of identity-relevant feature, we introduce a calibrated operation on the IN layer to enforce discriminative id-relevant information and filter out id-irrelevant information:

$$\begin{aligned} \tilde{\mathbf{R}}^I &= \text{CIN}(\mathbf{R}^I) \\ &= (\gamma \frac{\hat{\mathbf{R}}^I - \mu(\mathbf{R}^I)}{\sigma(\mathbf{R}^I)} + \beta) \cdot \text{Sigmoid}(\omega_v \odot \hat{\mathbf{R}}^I + \omega_o), \\ \hat{\mathbf{R}}^I &= \mathbf{R}^I + \omega_u \odot \text{pool}(\mathbf{R}^I), \end{aligned} \quad (8)$$

The CIN is utilized in pure id-relevant feature of CFD to enhance the instance-specific representations and filter out id-irrelevant information (*e.g.*, illumination, background,

Table 1. Performance (%) comparison with the state-of-the-art methods under Protocol-1. “MS” refers to the multiple training datasets, *i.e.*, Market-1501 (M), DukeMTMC-reID (D), CUHK-SYSU (CS), CUHK03 (C3) and CUHK02 (C2). We mark the results of the best results by **bold** text.

| Method | Type | Source | Target: VIPeR (V) | | | Target: PRID (P) | | | Target: GRID (G) | | | Target: iLIDS (I) | | | Mean of V,P,G,I | | |
|---------------------------|------|--------------|-------------------|-------------|-------------|------------------|-------------|-------------|------------------|-------------|-------------|-------------------|-------------|-------------|-----------------|-------------|-------------|
| | | | R1 | R5 | mAP | R1 | R5 | mAP | R1 | R5 | mAP | R1 | R5 | mAP | R1 | R5 | mAP |
| CDEL [25] | DG | M+C2+C3+CS+D | 38.5 | - | - | 57.6 | - | - | 33.0 | - | - | 62.3 | - | - | 47.9 | - | - |
| DIMN [32] | DG | M+C2+C3+CS+D | 51.2 | 70.2 | 60.1 | 39.2 | 67.0 | 52.0 | 29.3 | 53.3 | 41.1 | 70.2 | 89.7 | 78.4 | 47.5 | 70.1 | 57.9 |
| AugMining [34] | DG | M+C2+C3+CS+D | 49.8 | 70.8 | - | 34.3 | 56.2 | - | 46.6 | 67.5 | - | 76.3 | 93.0 | - | 51.8 | 71.9 | - |
| DualNorm [18] | DG | M+C2+C3+CS+D | 53.9 | 62.5 | 58.0 | 60.4 | 73.6 | 64.9 | 41.4 | 47.4 | 45.7 | 74.8 | 82.0 | 78.5 | 57.6 | 66.4 | 61.8 |
| DDAN [5] | DG | M+C2+C3+CS+D | 56.5 | 65.6 | 60.8 | 62.9 | 74.2 | 67.5 | 46.2 | 55.4 | 50.9 | 78.0 | 85.7 | 81.2 | 60.9 | 70.2 | 65.1 |
| RaMoE [7] | DG | M+C2+C3+CS+D | 56.6 | - | 64.6 | 57.7 | - | 67.3 | 46.8 | - | 54.2 | 85.0 | - | 90.2 | 61.5 | - | 69.1 |
| SNR [20] | DG | M+MT+C3+D | 55.1 | - | 65.0 | 49.0 | - | 60.0 | 30.4 | - | 41.3 | 91.9 | - | 87.0 | 56.6 | - | 63.3 |
| SNR [20] | DG | M+C2+C3+CS+D | 49.2 | - | 58.0 | 47.3 | - | 60.4 | 39.4 | - | 49.0 | 77.3 | - | 84.0 | 53.3 | - | 62.9 |
| CBN [53] | DG | M+C2+C3+CS+D | 49.0 | 63.4 | 59.2 | 61.3 | 73.8 | 65.7 | 43.3 | 48.4 | 47.8 | 75.3 | 84.6 | 79.4 | 57.2 | 67.6 | 63.0 |
| Person30K [1] | DG | M+C2+C3+CS+D | 53.9 | - | 60.4 | 60.6 | - | 68.4 | 50.9 | - | 56.6 | 79.3 | - | 83.9 | 61.1 | - | 67.3 |
| DIR-ReID [40] | DG | M+C2+C3+CS+D | 58.3 | 66.9 | 62.9 | 71.1 | 82.4 | 75.6 | 47.8 | 51.1 | 52.1 | 74.4 | 83.1 | 78.6 | 62.9 | 70.8 | 67.3 |
| MetaBIN [6] | DG | M+C2+C3+CS+D | 56.2 | 76.7 | 66.0 | 72.5 | 88.2 | 79.8 | 49.7 | 67.6 | 58.1 | 79.7 | 93.3 | 85.5 | 64.5 | 81.5 | 72.4 |
| QAConv ₅₀ [23] | DG | M+C2+C3+CS* | 57.0 | - | 66.3 | 52.3 | - | 62.2 | 48.6 | - | 57.4 | 75.0 | - | 81.9 | 58.2 | - | 67.0 |
| M ³ L [44] | DG | M+C2+C3+CS* | 60.8 | 75.6 | 68.2 | 55.0 | 79.0 | 65.3 | 40.0 | 64.0 | 50.5 | 65.0 | 83.3 | 74.3 | 55.2 | 75.5 | 64.6 |
| MetaBIN [6] | DG | M+C2+C3+CS* | 55.9 | - | 64.3 | 61.2 | - | 70.8 | 50.2 | - | 57.9 | 74.7 | - | 82.7 | 60.5 | - | 68.9 |
| CFD (Ours) | DG | M+C2+C3+CS* | 63.3 | 85.4 | 72.9 | 73.0 | 86.0 | 79.9 | 51.0 | 72.0 | 60.6 | 76.7 | 88.3 | 82.8 | 66.0 | 82.9 | 76.4 |

* We did not include DukeMTMC-reID [51] in the training domains since this dataset has been discredited by the creators. Although we used one less dataset, our method still has the best average performance on these four small datasets.

Table 2. Different evaluation settings of Protocol-1, Protocol-2 and Protocol-3.

| Setting | Training Data | Testing Data |
|------------|--|--------------------------|
| Protocol-1 | Com-(M+C2+C3+CS) | PRID, GRID, VIPeR, iLIDS |
| Protocol-2 | Com-(CS+C3+MT) Com-(M+CS+MT) Com-(M+CS+C3) | M C3 MT |
| Protocol-3 | CS+C3+MT M+CS+MT M+CS+C3 | M C3 MT |

viewpoints), towards better discriminative id-relevant information. Fig. 3 shows the details of the calibrated-and-standardized batch normalization and the calibrated instance normalization.

3.3. Overall Loss Function

To adequately learn discriminative feature representations, we propose to adaptive distill identity-relevant feature from the entangled feature and retribute it to the network to ensure high discrimination. Specifically, we add the ReID loss on the discriminative identity-relevant feature \mathbf{R}^I . Meanwhile, we also add a domain loss into the contributive domain-relevant features \mathbf{R}^D from the 4 ResNet blocks to ensure that id-irrelevant domain information does not flow into the subsequent network. The overall loss is as

$$\mathcal{L}_{Total} = \mathcal{L}_{ReID}(\mathbf{R}^I) + \sum_{i=1}^4 \lambda_i \cdot \mathcal{L}_{Domain}(\mathbf{R}_i^D). \quad (9)$$

where \mathcal{L}_{ReID} denotes the triplet loss and ID loss, \mathcal{L}_{Domain} denotes domain classification loss, and $\{\lambda_i\}_{i=1}^4$ denote hyper-parameters for balancing the losses.

4. Experiments

4.1. Datasets and Evaluation Settings

Due to the CVPR2022 General Ethical Conduct, we have taken down DukeMTMC [51] and adopted the new protocols based on the previous protocols [7, 18, 32, 34, 43] to evaluate the generalization ability of the model for person Re-ID.

Protocol-1: Following the previous methods [18, 32, 34], we employ the existing Re-ID benchmarks to evaluate the Re-ID model’s generalization ability. Specifically, the existing large-scale Re-ID datasets are viewed as multiple source domains, and the small-scale Re-ID datasets are used as unseen target domains. As shown in Tab. 2, seen domains include CUHK02 [21], CUHK03 [22], Market-1501 [49] and CUHK-SYSU [38]. Unseen domains contain VIPeR [12], PRID [15], GRID [26] and iLIDS [50]. All training sets and testing sets in the seen domains are used for model training. The four small-scale Re-ID datasets are tested respectively, where the final performances are obtained by the average of 10 repeated random splits of testing sets.

Protocol-2 and Protocol-3: Considering that the image quality of the small-scale Re-ID datasets is quite poor, the performances on these datasets can not precisely reflect the generalization ability of a model in real scenarios. The previous methods [7, 43] thus set two new kinds of protocols (*i.e.*, leave-one-out setting) for four large-scale Re-ID datasets. Specifically, four large-scale Re-ID datasets (Market-1501 [49], CUHK-SYSU [38], CUHK03 [22] and MSMT17 [36]) are divided into two parts: three datasets as the seen domains for training and the remaining one as the unseen domain for testing. In addition, for protocol-2, the test set of the seen domains also are adopted for training model, and protocol-3 only adopts the train set of seen domains for model training.

Table 3. Comparison with state-of-the-art domain generalization methods on four large-scale person ReID benchmarks under Protocol-2 and Protocol-3 — Market-1501 (M), Cuhk-SYSU (CS), CUHK03 (C3) and MSMT17 (MT). The performance is evaluated quantitatively by mean average precision (mAP) and cumulative matching characteristic (CMC) at Rank-1 (R1).

| Method | Source | IDs | Images | Market-1501 mAP R1 | | Source | IDs | Images | DukeMTMC mAP R1 | |
|--|--------------------|--------|---------|---|---|-------------------|--------|---------|--|---|
| SNR [20] QAConv ₅₀ [23] | Com-MT | 4,101 | 126,441 | 41.4 43.1 | 70.1 72.6 | Com-MT | 4,101 | 126,441 | 50.0 52.6 | 69.2 69.4 |
| QAConv ₅₀ [23]* SNR [20]* RDSBN [2] M ³ L (ResNet-50) [44] M ³ L (IBN-Net50) [44] | MT+D+C3 | 2,510 | 56,508 | 39.5 38.0 40.3 51.1 52.5 | 68.6 69.7 67.5 76.5 78.3 | MT+M+C3 | 2,559 | 52,922 | 43.4 36.0 - 48.2 48.8 | 64.9 56.5 - 67.1 67.2 |
| SNR [20]* M ³ L (ResNet-50) [44]* M ³ L (IBN-Net50) [44]* QAConv ₅₀ [44]* MetaBIN [6]* CFD (ResNet-50) | MT+CS+C3 | 13,742 | 72,190 | 34.6 58.4 61.5 63.1 57.9 70.0 | 62.7 79.9 82.3 83.7 80.0 87.2 | MT+M+C3 | 2,559 | 52,922 | - - - - - - | - - - - - - |
| SNR [20]* M ³ L (ResNet-50) [44] M ³ L (IBN-Net50) [44] RaMoE [7] | Com- (MT+D+C3) | 7,380 | 176,948 | 51.2 51.9 57.2 56.5 | 79.3 76.8 80.2 82.0 | Com- (MT+M+C3) | 7,069 | 169,956 | 50.3 51.3 54.1 56.9 | 69.6 69.1 71.9 73.6 |
| SNR [20]* M ³ L (ResNet-50) [44]* M ³ L (IBN-Net50) [44]* QAConv ₅₀ [44]* MetaBIN [6]* CFD (ResNet-50) | Com- (MT+CS+C3) | 17,502 | 175,111 | 52.4 61.2 62.4 66.5 67.2 79.1 | 77.8 81.2 82.7 85.0 84.5 91.8 | Com- (MT+M+C3) | 7,069 | 169,956 | - - - - - - | - - - - - - |
| Method | Source | IDs | Images | CUHK03 mAP R1 | | Source | IDs | Images | MSMT17 mAP R1 | |
| QAConv ₅₀ [23] | Com-MT | 4,101 | 126,441 | 22.6 | 25.3 | D | 702 | 16,522 | 8.9 | 29.0 |
| QAConv ₅₀ [23]* SNR [20]* M ³ L (ResNet-50) [44] M ³ L (IBN-Net50) [44] | MT+D+M | 2,494 | 62,079 | 19.2 12.2 30.9 31.4 | 22.9 12.1 31.9 31.6 | D+M+C3 | 2,220 | 36,823 | 10.0 9.3 13.1 15.4 | 29.9 27.0 32.0 37.1 |
| SNR [20]* M ³ L (ResNet-50) [44]* M ³ L (IBN-Net50) [44]* QAConv ₅₀ [44]* MetaBIN [6]* CFD (ResNet-50) | MT+CS+M | 13,762 | 77,761 | 8.9 20.9 34.2 25.4 28.8 36.9 | 8.9 31.9 34.4 24.8 28.1 36.9 | CS+M+C3 | 13,452 | 54,878 | 6.8 15.9 16.7 16.4 17.8 20.2 | 19.9 36.9 37.5 45.3 40.2 47.6 |
| SNR [20]* M ³ L (ResNet-50) [44] M ³ L (IBN-Net50) [44] RaMoE [7] | Com- (MT+D+M) | 7,414 | 192,271 | 26.2 32.9 34.4 33.5 | 26.8 34.5 35.0 34.6 | Com- (D+M+C3) | 4,780 | 79,926 | 13.9 15.2 17.2 13.5 | 36.9 36.2 39.9 34.1 |
| SNR [20]* M ³ L (ResNet-50) [44]* M ³ L (IBN-Net50) [44]* QAConv ₅₀ [44]* MetaBIN [6]* CFD (ResNet-50) | Com- (MT+CS+M) | 17,536 | 190,434 | 17.5 32.3 35.7 32.9 43.0 47.9 | 17.1 33.8 36.5 33.3 43.1 49.0 | Com- (CS+M+C3) | 14,902 | 78,089 | 7.7 16.2 17.4 17.6 18.8 25.4 | 22.0 36.9 38.6 46.6 41.2 54.1 |

[†] We re-implement this work based on the authors' code on Github with the same source datasets as us.

For simplicity, in the following sections, we denote Market1501 as M, CUHK02 as C2, CUHK03 as C3, MSMT17 as MT and CUHK-SYSU as CS. The three different evaluation settings are shown in Tab. 2.

4.2. Implementation Details

We adopt ResNet50 [13] as our backbone. Following the previous method [27], the last residual layer's stride size is set to 1. The generalized mean Pooling (GeM) [30] with a batch normalization layer is used after the backbone to obtain the Re-ID features. Images are resized to 384×128 , and the training batch size of each domain is set to 64, including 2 identities and 32 images per identity per domain. For data augmentation, we use random flipping, random cropping and color jittering. We train the model for

60 epochs. The learning rate is initialized as 3.5×10^{-4} .

4.3. Comparison to state-of-the-art methods

Comparison under the Protocol-1. As shown in Tab. 1, the training domains under the previous Protocol-1 setting include the five multiple source datasets (*i.e.*, M, D, C2, C3, and CS). However, due to ethical conduct, we must take away the DukeMTMC dataset from these four training domains since this dataset has been discredited by the creators, and adopt the remaining M, C2, C3, and CS as our training domains. Although we used one less dataset, our method still has the best average performance on these four small test datasets. Specifically, the mean performance of our CFD outperforms MetaBIN [6] by 1.5% R-1 accuracy and 4.0% mAP, and DIR-ReID [40] 3.1% R-1 accuracy and

Table 4. Ablation studies on CDM, CSBN and CIN. Models are trained with the other three datasets except the Market dataset.

| Backbone | CDM | CIN | CSBN | MT+CS+C3→M mAP | R1 |
|-----------|-----|-----|------|-------------------|--------------|
| ResNet-50 | Off | × | × | 53.98 | 75.27 |
| | Off | ✓ | × | 64.19 | 83.17 |
| | Off | × | ✓ | 62.15 | 81.81 |
| | Off | ✓ | ✓ | 66.63 | 84.78 |
| | On | × | × | 57.68 | 78.44 |
| | On | ✓ | × | 64.74 | 82.96 |
| | On | × | ✓ | 68.71 | 86.43 |
| | On | ✓ | ✓ | 69.98 | 87.18 |

7.3% mAP, respectively. When using the 4 datasets as the training domains, our CFD outperforms the 2nd competitor by 5.5% in terms of the R-1 mean performance accuracy.

Comparison under the Protocol-2 and the Protocol-3. As shown in Tab. 3, we compare the proposed CFD with MetaBIN [6], $QACovv_{50}$ [24], M^3L [43] and RaMoE [7] under Protocol-2 and Protocol-3. It is mentioned that we replace the DukeMTMC dataset with the CUHK-SYSU dataset, and re-implement some works based on the authors’ codes with the same source datasets. The results show that CFD outperforms the performances of these methods by a large margin. Specifically, our method improves the second-best $QACovv_{50}$ by 3.5% R1 accuracy and 6.9% mAP on Market-1501 under the Protocol-2. And under the setting of Protocol-3, our CFD also improves the second-best $QACovv_{50}$ by 6.8% and 12.6% in terms of R1 accuracy and mAP, respectively. The results demonstrate that the strong domain generalization of our CFD is attributed to calibrated feature decomposition with the guidance of calibrated normalization.

4.4. Ablation Study

Effectiveness of components in CFD. To investigate the effectiveness of each component in CFD, we conduct a series of ablation studies. As shown in Tab. 4, the performance of CFD without our designed normalization outperforms the baseline only by 3.17% R1 accuracy and 3.70% mAP. It indicates that vanilla attention mechanism can bring a slight improvement. Meanwhile, the model with CSBN/CSIN also can improve the performance by 8.17%/10.21% R1 accuracy and 6.54%/7.90% mAP respectively, which demonstrates the effectiveness of these two kinds of novel normalization technologies. Moreover, our proposed CDM with CIN and CSBN outperform the baseline by 11.91%/16.00% R1 accuracy and 6.54%/7.90% mAP, respectively. These results demonstrate that CDM with CIN and CSBN together can improve, even more, proving to be mutually beneficial. It also indicates that the CIN and CSBN can effectively guide CDM to enable better decomposition, which is integrated to fully exploit the effective information for improving the model generalization.

Influence of Disentanglement Design. In our designed CFD module, as described in Subsection 3.1, we use **a** and **b**

Table 5. Effectiveness of study on different decomposition strategy in the ResNet architecture.

| Method | R1 | MT+CS+C3→M R5 | R10 | mAP |
|-------------------|--------------|------------------|--------------|--------------|
| Baseline | 75.27 | 88.06 | 91.86 | 53.98 |
| PFD | 77.27 | 89.96 | 93.61 | 56.18 |
| CFD | 78.40 | 90.23 | 93.93 | 57.68 |
| Baseline+CIN+CSBN | 83.73 | 93.41 | 95.99 | 64.64 |
| PFD+CIN+CSBN | 85.04 | 94.24 | 96.14 | 65.98 |
| CFD+CIN+CSBN | 87.18 | 94.58 | 97.16 | 69.98 |

as masks to extract pure domain-relevant feature \mathbf{R}^- , entangled feature \mathbf{R}^* and pure id-relevant feature \mathbf{R}^+ from the residual feature \mathbf{F} . Here, we study the influence of different disentanglement designs. Following conventional disentanglement methods [10, 20, 40, 41], previous feature decomposition (PFD) methods directly disentangle the input feature \mathbf{F} into id-relevant feature \mathbf{R}^- and id-irrelevant/domain-related feature \mathbf{R}^+ . Tab. 5 shows the results. We observe that (1) without the designed normalization, our CFD outperforms PFD by **1.13%** and **1.5%** in Rank-1 and mAP for MT+CS+C3→M, respectively; (2) with the designed normalization, our CFD outperforms PFD by **2.18%/4.00%** in Rank-1 and mAP on the unseen Market1501, respectively. The results demonstrate that the designed CFD is beneficial for the feature decomposition from the perspective of improving model generalization. Meanwhile, these two normalization technologies and CFD complement each other to improve the model’s generalization.

5. Conclusion

In this paper, we propose a simple yet effective Calibrated Feature Decomposition module that focuses on improving the generalization capacity for person re-identification through a more judicious feature decomposition and reinforcement strategy. Specifically, we adopt the CSBN to learn calibrated person representation by jointly exploring intra-domain calibration and inter-domain standardization of multi-source domain features. CSBN restricts instance-level inconsistency of feature distribution for each domain and captures intrinsic domain-level specific statistics. Then, the above calibrated person representation is subtly decomposed into the identity-relevant feature, domain feature, and the remaining entangled one. For enhancing the generalization ability and ensuring high discrimination of identity-relevant features, a CIN is introduced to enforce discriminative id-relevant information and filter out id-irrelevant information, and meanwhile, the rich complementary clues from the remaining entangled feature are further employed to strengthen it.

6. Limitations and broader impact

As for positive impacts, we demonstrate that through extensive experiments that a suitable domain generaliz-

able method for person re-id contributes to performance on model generalization ability. We need not collect the images from the target domain and only use the existing data to train a robust model. Hence our domain generalization algorithm can have the potential to mitigate ethical concerns associated with the collecting of pedestrian data.

However, using a ReID system to identify pedestrians in a surveillance system may violate people’s privacy. Because ReID systems typically (but not always) rely on unauthorized surveillance data, not all human subjects were aware they were being recorded. As a result, governments and officials must go to great lengths to create stringent regulations and legislation governing the use of ReID technology.

A. Experiments

A.1. Ablation Study for Where to Add Which Normalization Strategy.

Table 6. Effectiveness of different normalization strategies in calibrated decomposition module.

| Calibrated Decomposition Module | | MT+CS+C3→M | |
|---------------------------------|-----------------------------------|--------------|--------------|
| Input Feature \mathbf{F} | pure ID Feature \mathbf{R}^+ | mAP | R1 |
| - | - | 57.68 | 78.44 |
| - | IN | 66.01 | 84.78 |
| BN | - | 58.08 | 79.08 |
| BN | IN | 65.51 | 84.00 |
| - | BN | 59.00 | 78.47 |
| IN | - | 65.15 | 84.53 |
| IN | BN | 65.15 | 83.94 |
| - | CSBN | 67.99 | 85.21 |
| CIN | - | 66.08 | 84.38 |
| CIN | CSBN | 69.00 | 86.97 |
| CSBN | - | 68.71 | 86.43 |
| CSBN | CSBN | 65.29 | 84.12 |
| - | CIN | 66.74 | 85.08 |
| BN | CIN | 66.62 | 85.14 |
| CBN | CIN | 69.27 | 86.89 |
| CSBN | IBN | 62.59 | 81.21 |
| CSBN | IN | 69.53 | 86.91 |
| CSBN | CIN | 69.98 | 87.18 |

To investigate the effectiveness of different normalization strategies in calibrated decomposition module, we conduct a series of ablation studies. We mainly adopt different normalization strategy (*i.e.*, BN, IN, CBN, IBN, CSBN, CIN) on the input \mathbf{F} and pure ID Feature \mathbf{R}^+ . Specifically, BN denotes to the batch normalization, IN denotes to the instance normalization, CBN refers to the calibrated BN [11],

IBN refers to the ibn-net [27]. CSBN and CIN are our designed normalization layer that is introduced in the Section 3.2 of manuscript paper. We observe that:

(1) As shown in Tab. 6, the performance of CFD without normalization only achieves 78.44% R1 accuracy and 57.68% mAP, respectively. It indicates that vanilla attention mechanism bring the slight improvement of model’s generalizable ability. Meanwhile, the widely used BN also has a negligible impact on performance.

(2) As we know, IN could filter out some instance specific style information from the content to enhance model’s generalizable ability. But the correct placement of IN is also not considered in the previous decoupling methods. As shown in Tab. 6, the experiments illustrate that putting IN on the ID feature performs better than the input feature by about 1%. The same conclusion is reached for the CSBN and CIN. These results demonstrate the importance of different types of normalization techniques placed in different positions on the corresponding features.

(3) Thanks to the compensation of the identity-relevant information through the proposed CIN, our CIN achieves superior generalization capability, which outperforms other instance normalization technologies (IN and IBN). Our designed CSBN also shows the better generalization capability by exploring jointly intra-domain calibration and inter-domain standardization, which outperforms other batch normalization technologies (BN and CBN). It is worth noting that after we add the CSBN into the ID feature \mathbf{R}^+ for replacing the CIN, the performance dropped slightly. This result illustrates that the right normalization layer should be placed in the right place.

(4) Moreover, the model with CSBN and CIN also can improve the performance by 8.74% R1 accuracy and 12.30% mAP respectively, which demonstrates the effectiveness of these two kinds of novel normalization technologies. These results demonstrate that CFD with CIN and CSBN together can improve, even more, proving to be mutually beneficial. It also indicates that the CIN and CSBN can effectively guide CFD to enable better decomposition, which is integrated to fully exploit the effective information for improving the model generalization.

A.2. Ablation Study for Where to Apply Calibrated Decomposition Module in the ResNet Architecture.

We compare the cases of adding a single CFD module to a different convolutional block/stage, and to all the four stages (*i.e.*, stage-1,2,3,4) of the ResNet-50 (see Tab. 7). The module is added after the last layer of a convolutional block/stage. As shown in Tab. 7, in comparison with Baseline, the improvement from adding CFD is significant on stage-2, stage-3 and stage-4 and is a little smaller on stage-1. When CFD is added to all the four stages, we achieve the

Table 7. Effectiveness of study on where to apply Calibrated Decomposition Module in the ResNet architecture.

| Method | CS+MT+C3→M | | | |
|----------|--------------|--------------|--------------|--------------|
| | R1 | R5 | R10 | mAP |
| Baseline | 75.27 | 88.06 | 91.86 | 53.98 |
| Stage-1 | 81.68 | 92.40 | 95.25 | 59.78 |
| Stage-2 | 82.13 | 92.58 | 95.10 | 62.00 |
| Stage-3 | 83.58 | 93.26 | 95.64 | 63.05 |
| Stage-4 | 82.81 | 93.08 | 95.61 | 64.54 |
| Stagesll | 87.18 | 94.58 | 97.16 | 69.98 |

best performance.

A.3. Ablation Study for Domain Loss.

Table 8. Effectiveness of domain loss on the CS+MT+C3→M setting. “B” refers to the baseline model.

| Method | CS+MT+C3→M | |
|------------------------------------|--------------|--------------|
| | R1 | mAP |
| B | 75.27 | 53.98 |
| B + Domain Loss | 77.01 | 55.94 |
| B + Domain Loss + CFD | 78.44 | 57.68 |
| B + CFD + CSBN + CIN | 84.80 | 63.45 |
| B + Domain Loss + CFD + CSBN + CIN | 87.18 | 69.98 |

As shown in Tab. 8, we investigate the influence of domain loss. We can observe that the Baseline model without domain loss obtain slight performance degradation over Baseline with domain loss. It demonstrates that the domain loss only brings the little improvement of model’s generalizable ability. Meanwhile, we can observe that the CFD model without domain loss obtains performance degradation over CFD with domain loss. It indicates that domain loss can help the CFD to perform feature decomposition.

A.4. Ablation Study for Attention Choices.

We conduct an ablation study on the types of adopted attention. As experimental results shown in Tab. 9, we find the SC is most effective for feature decomposition. While the spatial attention or channel-wise attention seem to be detrimental to the final performance. Although the best performance is based on the SC, we still adopt the channel attention in other experiment settings for fair comparisons. Because S is widely used on the disentanglement-based ReID task.

Table 9. Ablation study for attention type choices for feature decomposition. “S” denotes spatial attention in which a spatial mask of size $1 \times H \times W$ is learned. “C” denotes channel attention with a channel mask of size $C \times 1 \times 1$. “SC” denotes the joint using of both spatial attention and channel attention by multiplying them. We follow the implementations in CBAM [37].

| Methods | CS+MT+C3→M | | | |
|--------------------|------------|-------|-------|-------|
| | mAP | R1 | mAP | R1 |
| Baseline | 75.27 | 88.06 | 91.86 | 53.98 |
| Baseline+CFD w/ S | 81.21 | 91.39 | 94.03 | 58.16 |
| Baseline+CFD w/ C | 87.18 | 94.58 | 97.16 | 69.98 |
| Baseline+CFD w/ SC | 88.87 | 95.67 | 97.62 | 73.11 |

B. Visualization

B.1. Feature Map Visualization.

To better understand how a CFD module works, we visualize the intermediate feature maps of the fourth CFD module. Following [45, 52], we get each activation map by summarizing the feature maps along channels following with the min-max normalization.

Fig. 5 shows the activation maps of input feature \mathbf{F} , pure ID feature $\tilde{\mathbf{R}}^I$, and domain feature \mathbf{R}^D , respectively. Although the input feature \mathbf{F} mainly focus on foreground, there are still high response in the background and lack distinct salient responses. We can see that domain Feature \mathbf{R}^D has high response simultaneously on background and foreground. It demonstrates that some crucial characteristics are stubbornly entwined in both the domain-relevant interference and identity-relevant feature, which are intractable to decompose in an unsupervised manner. In contrast, the pure ID Feature $\tilde{\mathbf{R}}^I$ with the guidance of our designed normalization layers has high responses on salient regions of the human body, better capturing discriminative regions.

B.2. Feature t-SNE Visualization.

We analyze our CFD framework and baseline through the performance and t-SNE visualization from the 4-th CFD module. In the baseline, the four unseen target domains are largely separately distributed and have an obvious domain gap. Thank to the CFD module, this domain gap has been eliminated. Meanwhile, our method shows that our method has shorter distances between different domains than those of baseline. Thus, we demonstrate that our CFD framework is generalizable and practical for real-world situations.

References

- [1] Yan Bai, Jile Jiao, Wang Ce, Jun Liu, Yihang Lou, Xuetao Feng, and Ling-Yu Duan. Person30k: A dual-meta general-

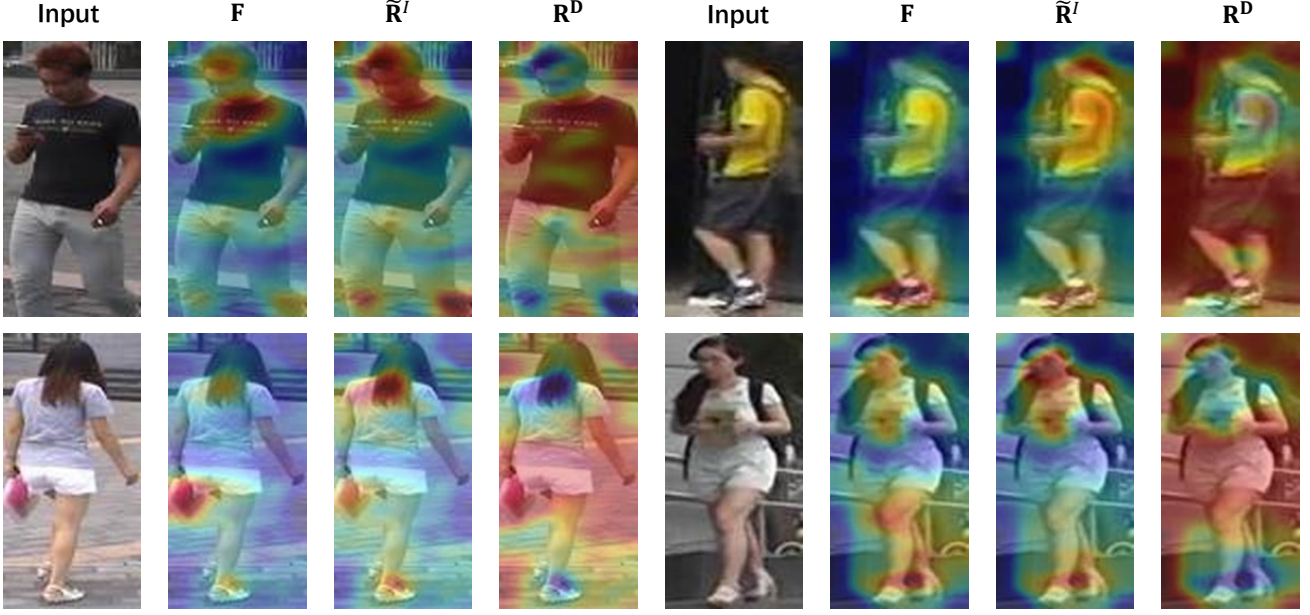


Figure 4. Activation maps of different features of input feature F , pure ID feature \tilde{R}^I , and domain feature R^D within a CFD module. They show that CFD can enhance the identity-relevant features (*i.e.*, pure ID feature \tilde{R}^I) well in the unseen target domain (*e.g.*, Market1501), towards improving model’s generalization ability. Meanwhile, There are still high responses of foreground on domain feature R^D . These results illustrates that some crucial characteristics are stubbornly entwined in both the domain-relevant interference and identity-relevant feature, which are intractable to decompose in an unsupervised manner.

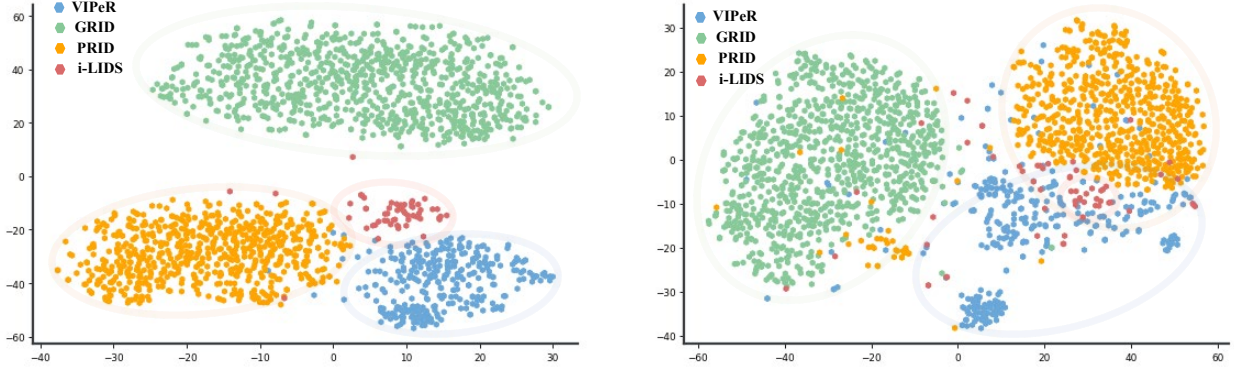


Figure 5. The t-SNE visualization of the embedding vectors on four unseen target datasets (VIPeR, PRID, GRID, and i-LIDS). Best viewed in color and shape.

- ization network for person re-identification. In *CVPR*, pages 2123–2132, 2021. [6](#)
- [2] Zechen Bai, Zhigang Wang, Jian Wang, Di Hu, and Errui Ding. Unsupervised multi-source domain adaptation for person re-identification. In *CVPR*, pages 12914–12923, June 2021. [7](#)
- [3] Woong-Gi Chang, Tackgeun You, Seonguk Seo, Suha Kwak, and Bohyung Han. Domain-specific batch normalization for unsupervised domain adaptation. In *CVPR*, 2019. [2](#)
- [4] Prithvijit Chattopadhyay, Yogesh Balaji, and Judy Hoffman. Learning to balance specificity and invariance for in and out of domain generalization. In *ECCV*, 2020. [1](#)
- [5] Peixian Chen, Pingyang Dai, Jianzhuang Liu, Feng Zheng, Qi Tian, and Rongrong Ji. Dual distribution alignment network for generalizable person re-identification. In *AAAI*, 2021. [6](#)
- [6] Seokeon Choi, Taekyung Kim, Minki Jeong, Hyungseob Park, and Changick Kim. Meta batch-instance normalization for generalizable person re-identification. In *CVPR*, 2021. [2](#), [3](#), [6](#), [7](#), [8](#)

- [7] Yongxing Dai, Xiaotong Li, Jun Liu, Zekun Tong, and Ling-Yu Duan. Generalizable person re-identification with relevance-aware mixture of experts. In *CVPR*, 2021. 2, 3, 6, 7, 8
- [8] Vincent Dumoulin, Jonathon Shlens, and Manjunath Kudlur. A learned representation for artistic style. *ICLR*, 2016. 5
- [9] Antonio D’Innocente and Barbara Caputo. Domain generalization with domain-specific aggregation modules. In *GCPR*, 2018. 2, 5
- [10] Chanho Eom and Bumsub Ham. Learning disentangled representation for robust person re-identification. *NIPS*, 32:5297–5308, 2019. 2, 3, 5, 8
- [11] Shang-Hua Gao, Qi Han, Duo Li, Ming-Ming Cheng, and Pai Peng. Representative batch normalization with feature calibration. In *CVPR*, pages 8669–8679, 2021. 2, 5, 9
- [12] Douglas Gray and Hai Tao. Viewpoint invariant pedestrian recognition with an ensemble of localized features. In *ECCV*, 2008. 6
- [13] Kaiming He, Xiangyu Zhang, Shaoqing Ren, and Jian Sun. Deep residual learning for image recognition. In *CVPR*, 2016. 3, 7
- [14] Lingxiao He, Wu Liu, Jian Liang, Kecheng Zheng, Xingyu Liao, Peng Cheng, and Tao Mei. Semi-supervised domain generalizable person re-identification. *arXiv preprint arXiv:2108.05045*, 2021. 2
- [15] Martin Hirzer, Csaba Beleznai, Peter M Roth, and Horst Bischof. Person re-identification by descriptive and discriminative classification. In *SCIA*, 2011. 6
- [16] Xun Huang and Serge Belongie. Arbitrary style transfer in real-time with adaptive instance normalization. In *ICCV*, pages 1501–1510, 2017. 2, 5
- [17] Zeyi Huang, Haohan Wang, Eric P Xing, and Dong Huang. Self-challenging improves cross-domain generalization. *arXiv preprint arXiv:2007.02454*, 2020. 1
- [18] Jieru Jia, Qiuqi Ruan, and Timothy M. Hospedales. Frustratingly easy person re-identification: Generalizing person re-id in practice. In *BMVC*, 2019. 6
- [19] Xin Jin, Cuiling Lan, Wenjun Zeng, and Zhibo Chen. Style normalization and restitution for domain generalization and adaptation. *TMM*, 2021. 3
- [20] Xin Jin, Cuiling Lan, Wenjun Zeng, Zhibo Chen, and Li Zhang. Style normalization and restitution for generalizable person re-identification. In *CVPR*, 2020. 2, 3, 4, 5, 6, 7, 8
- [21] Wei Li and Xiaogang Wang. Locally aligned feature transforms across views. In *CVPR*, 2013. 6
- [22] Wei Li, Rui Zhao, Tong Xiao, and Xiaogang Wang. Deepreid: Deep filter pairing neural network for person re-identification. In *CVPR*, 2014. 6
- [23] Shengcai Liao and Ling Shao. Interpretable and generalizable person re-identification with query-adaptive convolution and temporal lifting. In *ECCV*, pages 456–474. Springer, 2020. 6, 7
- [24] Shengcai Liao and Ling Shao. Interpretable and generalizable person re-identification with query-adaptive convolution and temporal lifting. In *ECCV*, 2020. 8
- [25] Ci-Siang Lin, Yuan-Chia Cheng, and Yu-Chiang Frank Wang. Domain generalized person re-identification via cross-domain episodic learning. *arXiv preprint arXiv:2010.09561*, 2020. 3, 6
- [26] Chen Change Loy, Tao Xiang, and Shaogang Gong. Multi-camera activity correlation analysis. In *CVPR*, 2009. 6
- [27] Hao Luo, Wei Jiang, Youzhi Gu, Fuxu Liu, Xingyu Liao, Shenqi Lai, and Jianyang Gu. A strong baseline and batch normalization neck for deep person re-identification. *TMM*, 2019. 7, 9
- [28] Massimiliano Mancini, Samuel Rota Buló, Barbara Caputo, and Elisa Ricci. Best sources forward: domain generalization through source-specific nets. In *ICIP*, 2018. 2, 3
- [29] Vihari Piratla, Praneeth Netrapalli, and Sunita Sarawagi. Efficient domain generalization via common-specific low-rank decomposition. In *ICML*, 2020. 2
- [30] Filip Radenović, Giorgos Tolias, and Ondřej Chum. Fine-tuning cnn image retrieval with no human annotation. *TPAMI*, 2018. 7
- [31] Seonguk Seo, Yumin Suh, Dongwan Kim, Geeho Kim, Jongwoo Han, and Bohyung Han. Learning to optimize domain specific normalization for domain generalization. In *ECCV*, 2020. 2, 3
- [32] Jifei Song, Yongxin Yang, Yi-Zhe Song, Tao Xiang, and Timothy M Hospedales. Generalizable person re-identification by domain-invariant mapping network. In *CVPR*, 2019. 2, 3, 6
- [33] Chi Su, Jianing Li, Shiliang Zhang, et al. Pose-driven deep convolutional model for person re-identification. In *ICCV*, 2017. 1
- [34] Masato Tamura and Tomokazu Murakami. Augmented hard example mining for generalizable person re-identification. *arXiv preprint arXiv:1910.05280*, 2019. 6
- [35] Dmitry Ulyanov, Andrea Vedaldi, and Victor Lempitsky. Improved texture networks: Maximizing quality and diversity in feed-forward stylization and texture synthesis. In *CVPR*, pages 6924–6932, 2017. 5
- [36] Longhui Wei, Shiliang Zhang, Wen Gao, and Qi Tian. Person transfer gan to bridge domain gap for person re-identification. In *CVPR*, 2018. 6
- [37] Sanghyun Woo, Jongchan Park, Joon-Young Lee, and In So Kweon. Cbam: Convolutional block attention module. In *ECCV*, pages 3–19, 2018. 10
- [38] Tong Xiao, Shuang Li, Bochao Wang, Liang Lin, and Xiaogang Wang. Joint detection and identification feature learning for person search. In *CVPR*, 2017. 6
- [39] Li Zhang, Tao Xiang, and Shaogang Gong. Learning a discriminative null space for person re-identification. In *CVPR*, 2016. 1, 5
- [40] Yi-Fan Zhang, Hanlin Zhang, Zhang Zhang, Da Li, Zhen Jia, Liang Wang, and Tieniu Tan. Learning domain invariant representations for generalizable person re-identification. *arXiv preprint arXiv:2103.15890*, 2021. 2, 3, 6, 7, 8
- [41] Zhizheng Zhang, Cuiling Lan, Wenjun Zeng, Quanzeng You, Zicheng Liu, Kecheng Zheng, and Zhibo Chen. Disentanglement-based cross-domain feature augmentation for effective unsupervised domain adaptive person re-identification. *arXiv preprint arXiv:2103.13917*, 2021. 2, 3, 4, 8

- [42] Haiyu Zhao, Maoqing Tian, Shuyang Sun, et al. Spindle net: Person re-identification with human body region guided feature decomposition and fusion. In *CVPR*, 2017. 1
- [43] Yuyang Zhao, Zhun Zhong, Fengxiang Yang, Zhiming Luo, Yaojin Lin, Shaozi Li, and Nicu Sebe. Learning to generalize unseen domains via memory-based multi-source meta-learning for person re-identification. In *CVPR*, 2021. 2, 3, 6, 8
- [44] Yuyang Zhao, Zhun Zhong, Fengxiang Yang, Zhiming Luo, Yaojin Lin, Shaozi Li, and Nicu Sebe. Learning to generalize unseen domains via memory-based multi-source meta-learning for person re-identification. In *CVPR*, pages 6277–6286, 2021. 6, 7
- [45] Kecheng Zheng, Cuiling Lan, Wenjun Zeng, Jiawei Liu, Zhizheng Zhang, and Zheng-Jun Zha. Pose-guided feature learning with knowledge distillation for occluded person re-identification. In *ACM MM*, pages 4537–4545, 2021. 10
- [46] Kecheng Zheng, Cuiling Lan, Wenjun Zeng, Zhizheng Zhan, and Zheng-Jun Zha. Exploiting sample uncertainty for domain adaptive person re-identification. In *AAAI*, 2021.
- [47] Kecheng Zheng, Wu Liu, Lingxiao He, Tao Mei, Jiebo Luo, and Zheng-Jun Zha. Group-aware label transfer for domain adaptive person re-identification. In *CVPR*, pages 5310–5319, 2021. 1
- [48] Kecheng Zheng, Wu Liu, Jiawei Liu, Zheng-Jun Zha, and Tao Mei. Hierarchical gumbel attention network for text-based person search. In *ACM MM*, pages 3441–3449, 2020.
- [49] Liang Zheng, Liyue Shen, Lu Tian, Shengjin Wang, Jingdong Wang, and Qi Tian. Scalable person re-identification: A benchmark. In *ICCV*, 2015. 6
- [50] Wei-Shi Zheng, Shaogang Gong, and Tao Xiang. Associating groups of people. In *BMVC*, 2009. 6
- [51] Zhedong Zheng, Liang Zheng, and Yi Yang. Unlabeled samples generated by gan improve the person re-identification baseline in vitro. In *ICCV*, 2017. 6
- [52] Kaiyang Zhou, Yongxin Yang, Andrea Cavallaro, and Tao Xiang. Omni-scale feature learning for person re-identification. In *CVPR*, pages 3702–3712, 2019. 10
- [53] Zijie Zhuang, Longhui Wei, Lingxi Xie, Tianyu Zhang, Hengheng Zhang, Haozhe Wu, Haizhou Ai, and Qi Tian. Rethinking the distribution gap of person re-identification with camera-based batch normalization. In *ECCV*, pages 140–157. Springer, 2020. 2, 3, 6
- [54] Yang Zou, Xiaodong Yang, Zhiding Yu, Bhagavatula Vijayakumar, and Jan Kautz. Joint disentangling and adaptation for cross-domain person re-identification. In *ECCV*, 2020. 2, 3